

Contents lists available at ScienceDirect

Fuel

journal homepage: www.elsevier.com/locate/fuel



Full Length Article



Influence of catalyst agglomerate internal structure on PEFC performance investigated by a multiscale numerical model

J. Tian^a, M.S. Ismail^b, K.J. Hughes^{a,*}, D.B. Ingham^a, L. Ma^a, M. Pourkashanian^a

ARTICLE INFO

Keywords:
Polymer electrolyte fuel cells
Catalyst layer
Multiscale model
Agglomerate model

ABSTRACT

A multiscale modeling framework, which consists of catalyst agglomerate scale and fuel scale models, has been developed for polymer electrolyte fuel cells (PEFCs). The performance of the agglomerate model is numerically linked to the fuel cell model by employing an interpolation function that represents the performance of the agglomerate. This framework unlocks the restrictions associated with the conventional agglomerate PEFC model by allowing the user to freely investigate the impact of the structure and the composition of the catalyst agglomerate. Thus the impact of the internal structure of the catalyst agglomerate on the fuel cell performance has been investigated. The results have shown that the fuel cell performs better with catalyst agglomerates embodying "separate" active clusters and this impact becomes more profound as the size of the agglomerate increases. Also, it has been shown that the performance of the catalyst agglomerate becomes significantly better as the agglomerate size decreases. These outcomes and other outcomes have been presented and fully discussed.

1. Introduction

Polymer electrolyte fuel cells (PEFCs) are promising power conversion technologies and this is due to their high efficiency (~50 %), low operating temperatures (typically between 20 and 80 °C) and ease of construction [1–6]. However, PEFCs experience some voltage losses that impact their widespread commercialization, one of which is the activation voltage losses which are mainly caused by the slow kinetics of the oxygen reduction reaction taking place at the cathode electrode and the low utilization of conventional platinum-based catalysts [7-9]. The catalyst layer is a porous structure that consists of platinum, carbon black and ionomers [10-12,12,13]. Clearly, the use of precious platinum in PEFCs needs to be optimized to reduce the cost and increase the catalyst utilization at the same time. Many researches have shown that increasing the specific area can maximize the utilization of the catalyst and subsequently the fuel cell performance; this could be achieved by employing nano-manufacturing methods [14,15]. Optimizing catalyst loading through only experimental means is costly and time-consuming. On the other hand, adopting mathematical modelling-aided experimentation saves a considerable amount of time and cost, especially when considering the increasingly improved accuracy of the numerical models [16-20].

Significant advancements in the microstructures of cathode catalyst layers (CLs) began in the early 1990 s [21]. Mathematical modelling and the associated parametric studies of the catalyst layers started in early 2020 s [22-24]. It turns out that there have been two commonly used models for PEFC catalyst layers: (i) homogeneous and (ii) agglomerate models. Homogeneous models assume that the catalyst layer is a porous layer composed of a uniform mixture of ionomers, platinum, and carbon; see for example [25-28]. In addition, homogeneous models could resolve the spatial variation of the key variables within the catalyst layer. However, they do not capture the impact of the microstructure of the catalyst. On the other hand, the agglomerate models assume that the catalyst layer is typically composed of uniformly distributed spherical agglomerates covered by ionomers, and these spherical agglomerates are composed of a mixture of ionomers, carbon, and platinum; see for example [29-33,30]. This structure overcomes the shortcomings of the homogenous model as it accounts for the dissolution of the reactant gas in the ionomer phase and reasonably captures the effects of the catalyst microstructure on the fuel cell performance. Many studies have shown that the simulation results of this agglomerate model are more consistent with the experimental results [27,34,35]. The agglomerate model has been used to investigate the influence of the shape and the size of the catalyst agglomerate on the performance of the fuel cells. Jain et al. [29] developed a two-dimensional model to study the influence of the shape

E-mail address: k.j.hughes@sheffield.ac.uk (K.J. Hughes).

^a Energy 2050, Department of Mechanical Engineering, Faculty of Engineering, University of Sheffield, Sheffield S3 7RD, United Kingdom

^b School of Engineering, University of Hull, Hull HU6 7RX, United Kingdom

^{*} Corresponding author.

| Nomenclature | | Subscripts (Unless stated otherwise, all the subscripts in this thesis are | |
|----------------|---|--|------------------------------|
| | | given as | follows:) |
| a | Specific surface area of platinum catalyst, m^{-1} | agg | Agglomerate |
| a_{agg} | Specific surface area of agglomerate, m ⁻¹ | cl | Catalyst layer |
| A_{pt} | Electrochemical surface area of platinum catalyst, $m^2 kg^{-1}$ | eff | effective |
| C_j | Concentration of species j, kg m ⁻³ | mem | Membrane |
| Ď | Diffusivity, m ² /s | pt | Platinum |
| F | Faraday constant, C/mol | S | Solid phase |
| H | Henry's constant, atm m ³ mol ⁻¹ | 1 | Electrolyte phase |
| i | Current density, $A/m^{-2}(- -)$ | k | Species k |
| L | Thickness, μm | 0 | Reference |
| M_k | Molecular weight of species k, kg mol ⁻¹ | | |
| P | Pressure, Pa | Abbreviations | |
| R | Universal gas constant, Pa.m ³ mol ⁻¹ K ⁻¹ | GDL | Gas diffusion layer |
| R _i | Reaction rate of reactant i, mol m ⁻³ s ⁻¹ | MEA | Membrane electrode assembly |
| Ť | Temperature, K | PEFC | Polymer electroyte fuel cell |
| V | Volume, m ³ | Chemical symbols | |
| Greek symbols | | CO_2 | Carbon dioxide |
| α | Charge transfer coefficient, – | H^{+} | Proton |
| ε | Porosity, – | H_2 | Hydrogen molecule |
| e Ø | Potential, V | H_2O | Water molecule |
| | Overpotential, V | O_2 | Oxygen molecule |
| η | Density, kg/m ³ | _ | •• |

of the agglomerate on the fuel cell performance. They found that the fuel cell performance is highly sensitive to the agglomerate shape (spherical, plate-like or cylindrical) and that it is significantly enhanced when the size of the agglomerates is reduced.

Recently, very few multiscale PEFCs that numerically link the performance of the catalyst agglomerate to the performance of the fuel cell have been developed. The advantages of these models are that they are flexible and, with them, one could freely investigate the effects of the composition, the structure, and the shape of the catalyst agglomerate. In other words, the user of the multiscale model is not limited to the three basic shapes (spherical, plate-like, or cylindrical) as is the case in the conventional agglomerate model. What follows are the very few studies that have been performed on the multiscale PEFC models. Kamarajugadda and Mazumder [36] developed a flooded agglomerate model and coupled it with a two-dimensional fuel cell model to investigate the influence of overlapping agglomerates and agglomerates of different sizes on the performance of the fuel cells. Their research found that the shape of the agglomerates has minimal effect on the fuel cell performance when the size of the agglomerates is small (e.g. 100 nm), but has a significant impact when the size of the agglomerates is large (e.g. 1000 nm). Moore et al. [37] developed a multi-scale model that coupled a 1D catalyst agglomerate model with a 2D fuel cell model. They found that the properties of the agglomerates (e.g. proton conductivity) could significantly affect the current density within the catalyst layer and ultimately impact the performance of the fuel cell. Ismail et al. [10] developed a multiscale model to study the effect of the catalyst agglomerate shape on the fuel cell performance. Firstly, the threedimensional agglomerate model was solved, and then the results (in the form of volumetric current density as a function of the dissolved oxygen concentration and activation overpotential) were numerically coupled with a 1D fuel cell cathode model. Their study found that the fuel cell performance is a maximum with a cylindrical catalyst agglomerate and this is due to the relatively high specific surface area demonstrated by this shape. Mu et al. [38] developed a multiscale model, incorporating a microscale model alongside a fuel cell scale model, to investigate species transport and electron transfer. Their findings revealed that the pores play a crucial role in determining the limiting current density. Dou et al. [22] developed a pore-scale model to investigate how the structure of the catalyst layer influences the performance of PEM fuel cells. Their research demonstrates that a reasonable carbon aggregation rate can enhance both reactant transportation and catalyst performance.

Notably, the above-mentioned multiscale PEFC models assumed that the active area, which consists of the catalysts and the ionomer, within the catalyst agglomerate is uniform. However, the micrographs of the catalyst layer show that this is mostly not the case: the catalyst agglomerate consists of separate, contacting, and/or overlapping active regions and non-active regions which mostly consist of the ionomer phase and/or pores [39–41]. Therefore, the objective of this study is to investigate the influence of the internal structure of the catalyst agglomerate on the fuel cell performance. To achieve this objective, a multiscale PEFC modeling framework has been developed. Within this framework, the performance of a three-dimensional agglomerate model is numerically linked to the performance of a one-dimensional PEFC model. Further, the sensitivity of the outcomes of the modeling framework to the size of the catalyst agglomerate has been also investigated.

2. Model description

Two numerical models that vary in length scale have been developed to study the influence of the internal structure of the catalyst agglomerate on the PEFC performance. The first model is a nanoscale/microscale catalyst agglomerate (the right image shown in Fig. 1) and the other model is a macroscale PEFC model (the left image shown in Fig. 1). In the catalyst agglomerate model, the active clusters (blue areas in Fig. 1 right) are assumed to consist of a uniform mixture of the catalyst, specifically platinum nanoparticles supported on carbon particles mixed with the ionomer. In contrast, the non-active regions (white areas in Fig. 1 right) are assumed to be purely ionomer. The fuel cell is assumed to operate under isothermal and low-humidity conditions in order to isolate the thermal and saturation effects. This is a common practice in fuel cell modelling in order to focus on the area of interest which is in this case the internal structure of the catalyst agglomerate. The catalyst agglomerate model is numerically linked to the PEFC-scale model to investigate the effects of its internal structure on the fuel cell performance [42]. The following two subsections describe each model and

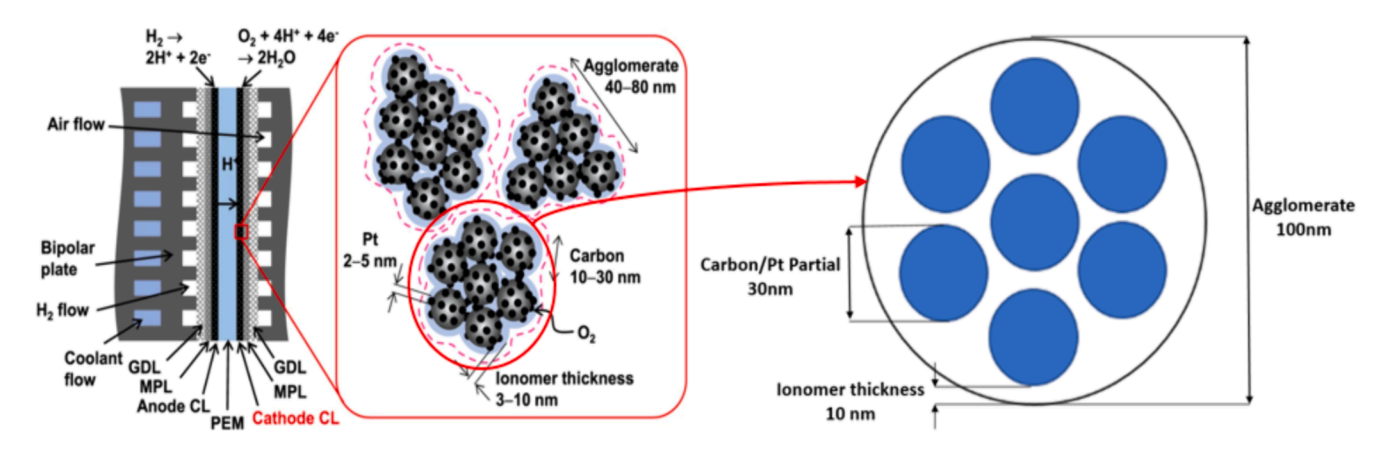


Fig. 1. A schematic showing the multi-scale structure of the catalyst layer [41].

detail the governing equations for each one.

2.1. Microscale model of the catalyst agglomerate

Consulting Fig. 1 and other related micrographs [43–45], the catalyst agglomerate in this study is assumed to be spherical and consists of spherical active clusters and non-active regions. The active clusters (red areas in Fig. 2) are assumed to comprise a uniform mixture of the catalyst (i.e. platinum nanoparticles supported on carbon particles and the ionomer) while the non-active region (grey areas in Fig. 2) was assumed to be purely ionomer. For simplicity, the active clusters are assumed to be identical, and they are either: (i) separate from each other, (ii) contacting each other or (iii) overlapping with each other; see Fig. 2. Note that the catalyst agglomerate may contain more than one internal structure; it may contain for example "separate" and "contacting" active clusters. However, for simplicity and to meet the objective of this study, which is to show the impact of ignoring the internal structure of the catalyst agglomerate, the cases investigated were limited to the above "simplified" structures. In all the structures, the minimum distance between the active clusters and the outer surface of the agglomerate was assumed to be one-tenth of the radius of the agglomerate; for example, if the radius of the agglomerate is 100 nm, then this distance is 10 nm [10]. It should be noted that, due to symmetry, only one-eighth of the catalyst agglomerate was considered to save computational time.

The following are the equations used to simulate the physics in the catalyst agglomerate. The reactant gas (i.e. oxygen in this case) is realistically assumed to be transported within the agglomerate by diffusion (i.e. other modes of transport such as convection are practically assumed to be negligible) and reacts in the active clusters of the agglomerate [46]:

$$\nabla D_e^{\text{eff}} \nabla C_{O_2} - R_{\text{exn},O_2} = 0 \tag{1}$$

where C_{O_2} is the molar concentration of the dissolved oxygen and ∇D_e^{eff}

is the effective diffusivity of the dissolved oxygen in the ionomer phase which is obtained using the Bruggeman correlation [26]:

$$D_e^{\text{eff}} = \begin{cases} D_e \\ \varepsilon_e^{1.5} D_e \end{cases} \text{ in the non - active region}$$
in the active clusters

where D_e is the diffusivity of the dissolved oxygen in the ionomer and ε_e is the volume fraction of the ionomer phase in the active region. R_{exn,O_2} is the oxygen molar consumption:

$$R_{exn,O_2} = \begin{cases} 0 & \text{in the non - active region} \\ kC_{O_2} & \text{(3)} \end{cases}$$

in the active clusters

$$k = \frac{i_0 a}{4FC_{O_2}^{ref}} \exp\left(\frac{-\alpha F}{RT}\eta\right) \tag{4}$$

where k is the reaction rate constant, i_0 is the exchange current density, F is the Faraday's constant, $C_{O_2}^{ref}$ is the reference concentration of the dissolved oxygen, α is the charge coefficient, T is the temperature, R is the universal gas constant, η is the activation over-potential which is one of the input variables for the model, and α is the specific surface area of the catalyst [47]:

$$a = \frac{l_{pt} A_{pt}}{L_{cl}} \tag{5}$$

where l_{pt} is the platinum loading, A_{pt} is the electrochemical surface area of the platinum catalyst and L_{cl} is the thickness of the catalyst layer. The average current density of the agglomerate $\overline{I_{agg}}$ is calculated using Faraday's law:

$$\overline{I_{agg}} = 4Fk\overline{C_{O_2}} \tag{6}$$

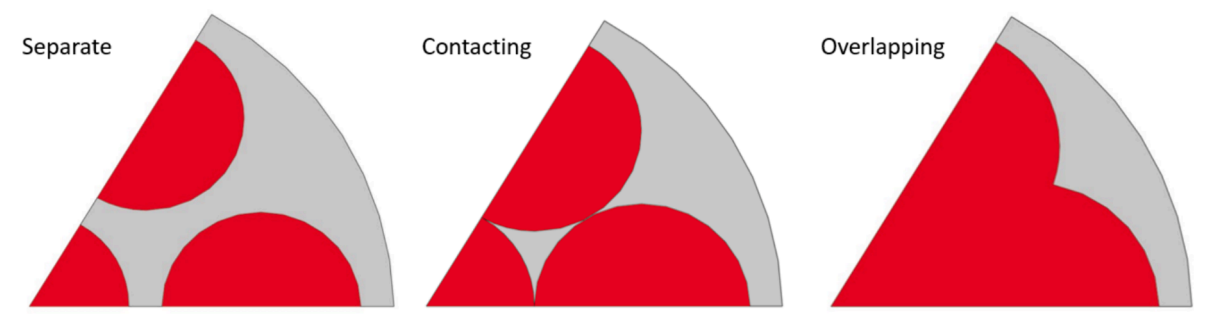


Fig. 2. A schematic showing various possible internal structures of the agglomerate.

where $\overline{C_{O_2}}$ is the average concentration in the active clusters. It is worth to note that, from Equations (4) and (6), the relationship between the local current density and the local activation overpotential is exponentially proportional. The boundary conditions used to solve Equation (1) are shown in Fig. 3. Constant dissolved oxygen concentration ($C_{O_2,0}$) is used for the surface of the agglomerate and zero flux of the dissolved oxygen concentration ($\nabla C_{O_2} = 0$) is used for the symmetrical lines in the computational domain.

In order to solve Equation (1), COMSOL Multiphysics 6.0 was used and the iterative linear solver GMRES (Generalised Minimum Residual) was applied. A mesh independence study was performed. Namely, the maximum mesh size was decreased from 0.003 to 0.0003 μm and the average current density was found to change by less than 1 %. Hence, the mesh with a maximum mesh size of 0.003 μm was used. For this mesh, the number of elements was found to be around 110 K; Fig. 4 shows a meshed 2D cut of the modeled catalyst agglomerate with separate active clusters. The computational time required for generating the mesh and solving the model was, using an Intel Xeon 3.80 GHz processor, about 60 min.

2.2. Macroscale PEFC model

Fig. 5 shows a schematic for the one-dimensional PEFC model with the boundary conditions used to solve the model (the boundary conditions will be revisited at the end of this section). For simplicity, the fuel cell is assumed to operate under isothermal and low-humidity conditions to isolate the thermal and saturation effects. To this end, the only governing equations considered are the conservation equations of chemical species and charge. What follows are the governing equations used in the model.

The continuity equation is given by:

$$\nabla \bullet (\rho \overrightarrow{u}) = 0 \tag{7}$$

where \overrightarrow{u} is the velocity vector and ρ is the density of the gaseous mixture. The conservation of species equations is obtained using the following equation:

$$\rho(\overrightarrow{u} \bullet \nabla) = -\nabla(j_i) + R_i \tag{8}$$

where j_i is the mass flux relative to the mass averaged velocity of species i, and R_i is the source term representing the production or consumption rate. j_i is defined as follows [10]:

$$j_{i} = -\rho \omega_{i} \sum_{k} D_{ik}^{\text{eff}} \frac{M}{M_{k}} (\nabla \omega_{k} + \omega_{k} \frac{\nabla M}{M})$$

$$(9)$$

where ω_i is the mass fraction of the species i, $D_{ik,eff}$ is the effective

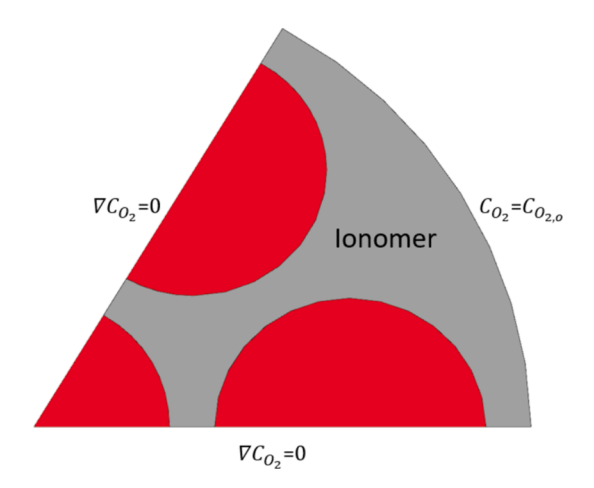


Fig. 3. The boundary conditions used for the agglomerate model.

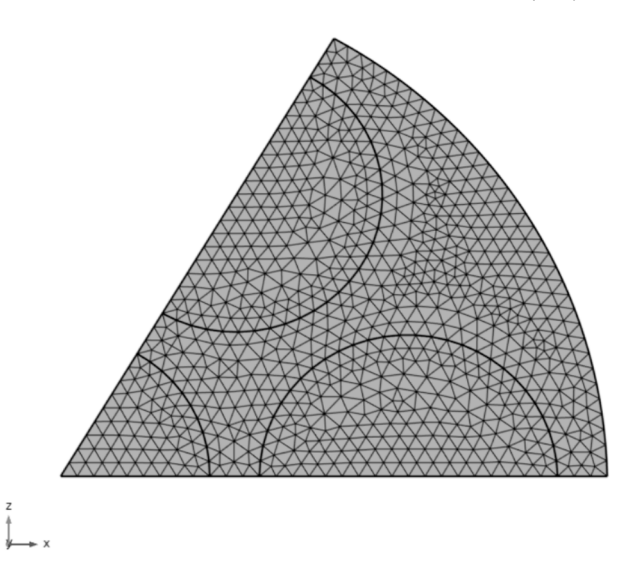


Fig. 4. A 2D meshed cut of the modeled catalyst agglomerate.

diffusivity of the chemical species i (e.g. oxygen) into the chemical species k (e.g. nitrogen). For ideal gas mixtures, the density is given by:

$$\rho = \frac{pM}{RT} \tag{10}$$

where p is the absolute pressure. The molecular weight of the gas mixture, M, is given by:

$$M = \sum \chi_i M_i \tag{11}$$

where χ_i and M_i are the mole fraction and the molar mass of the chemical species i, respectively. $D_{ik,eff}$ in the GDL or the catalyst layer (CL) is calculated by:

$$D_{ik,eff} = \begin{cases} 0.008e^{4.81e} D_{ik} in the GDLs \\ e^{1.5} D_{ik} in the CLs \end{cases}$$
 (12)

where ε is the porosity. The source term R_i shown in Equation (8) is given by:

$$R_i = \frac{I}{nF} \tag{13}$$

where n is the number of electrons transferred in the reaction (4 for oxygen and 2 for hydrogen and water), I is the local volumetric current density which is computed by making use of the outcomes of the agglomerate scale model as will be shown later in this section. The water vapor is calculated by:

$$S_{H_2o} = 2R_i + nd\nabla \bullet i/F \tag{14}$$

where *nd* is the drag coefficient. The conservation of charge equations is given by:

$$\nabla(-\sigma_s \nabla \phi_s) = \nabla \bullet i \tag{15}$$

$$\nabla(-\sigma_l \nabla \phi_l) = -\nabla \bullet i \tag{16}$$

where σ_s and σ_l are the electrical conductivity and the ionic conductivity of the solid phase and ionomer phase, respectively, and ϕ_s and ϕ_l are the solid-phase and the ionomer-phase potentials, respectively. Note that Equation (15) applies to the GDLs and the CLs while Equation (16) is applicable to the CL and the membrane electrolyte. The local activation over-potential η in the cathode catalyst layer, η_c , is given by:

$$\eta_c = \phi_s - \phi_l - E_{eq} \tag{17}$$

Fig. 5. A schematic diagram of the PEFC model and the boundary conditions used.

where E_{eq} is the theoretical cell potential which was calculated using the Nernst equation [46] and found to be 1.221 V. The local activation overpotential in the anode catalyst layer, η_a , is given by:

$$\eta_a = \phi_s - \phi_l \tag{18}$$

The local volumetric current density within the cathode catalyst layer, I_c , is computed using the following equation [10]:

$$I_c = \overline{I_{agg}}(1 - \varepsilon_{cl}) \tag{19}$$

where $\overline{I_{agg}}$ is the average volumetric current density of the modeled agglomerate which is obtained using Equation (6) and ε_{cl} is the porosity of the catalyst layer. Note that I_c changes with cathode activation overpotential and concentration of dissolved oxygen; therefore, $\overline{I_{agg}}$ is repeatedly solved for using a realistic set of cathode activation overpotential (ranging between -0.1 and -1 V) and concentration of dissolved oxygen (ranging between 0 and 0.86 mol/m³) [9]. The resulting $\overline{I_{agg}}$ values are then used as an interpolation function to compute I_c ; Fig. 6 shows a typical interpolation function for the agglomerate volumetric current density, I_a , is obtained using the following conventional form of Butler-Volmer equation:

$$I_{a}=i_{o}a\left(exp\left(\frac{\alpha_{a}F\eta_{a}}{RT}\right)-exp\left(\frac{-\alpha_{c}F\eta_{a}}{RT}\right)\right) \tag{20}$$

where i_o is the reference exchange current density of a unit active surface area, a is the specific surface area, which is calculated by Equation (5), α_a and α_c are the anodic and cathodic charge transfer coefficients and η_a is the anodic activation overpotential which is calculated by Equation

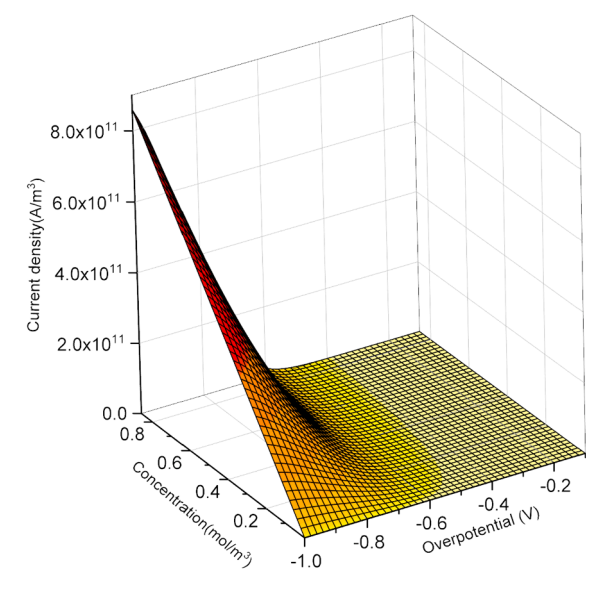


Fig. 6. A typical plot for the interpolation plot of volumetric current density as a function of dissolved oxygen concentration and activation overpotential for a modeled agglomerate with 100 nm radius and separate active clusters.

(18). For a given cell potential, the local cathodic or anodic volumetric current density is averaged over the length of the catalyst layer and multiplied by this length to obtain a point in the polarisation curve. Fig. 5 shows the boundary conditions used to solve the model.

Concentration boundary conditions were prescribed at the left and the right sides of the computational domain. Likewise, solid phase potential was prescribed at the left and right sides of the computational domain; it equals the cell potential at the outermost point of the cathode GDL and equals zero at the outermost point of the anode GDL. On the other hand, zero-flux ionomer-phase boundary conditions were used at the outermost points of the catalyst layers. The governing equations (7), (8), (15), and (16) were solved using COMSOL Multiphysics® 6.0. The solver employed for this task was MUMPS, which is a sparsely direct and massively parallel linear system solver. The domain was discretized, with a focus on refining the mesh near the interface between the catalyst layer and the GDL until a solution that was independent of mesh size was obtained. The maximum element size was set to 0.012 µm, and a maximum element growth rate of 1.2 was used. This choice was made to prevent unstable behavior in the high current density region of the polarisation curve. The solution-independent mesh consisted of approximately 125 elements. Table 1 shows the parameters used to solve the agglomerate scale and the fuel cell scale models.

3. Results and discussion

In order to validate the current multi-scale model, the output from this modeling framework (in the form of a polarisation curve) needs to be compared with the corresponding output generated from the conventional model in which the effects of the catalyst agglomerate are analytically coupled. Assuming spherical agglomerates, the cathodic current density used in the verification is given by [36,37]:

$$\nabla \bullet i_c = 4F(1 - \varepsilon_{cl})C_{O_2,o} \frac{r_{agg}^3}{\left(r_{agg} + \delta_{agg}\right)^3} \left(\frac{1}{E_r k} + \frac{r_{agg}\delta_{agg}}{a_{agg}(r_{agg} + \delta_{agg})D_e}\right)^{-1}$$
(21)

where $C_{O_2,o}$ is the specified dissolved oxygen concentration at the surface of the ionomer film and can be calculated using the following expression:

$$C_{O_2,o} = \frac{C_{O_2,g}RT}{H} \tag{22}$$

Where $C_{O_2,g}$ is the concentration of gas phase oxygen before being dissolved into the surface of the ionomer film, H is Harry's constant. The specific surface area of the spherical agglomerate a_{agg} is given by [20]:

$$a_{\rm agg} = \frac{3}{r_{\rm agg}} \tag{23}$$

where r_{agg} is the radius of the agglomerate which is, in this validation case, 100 nm. The effectiveness factor of the spherical agglomerate E_r used in Equation (21) is given as follows [49,46]:

$$E_r = \frac{1}{\Phi_L} (\frac{1}{\tanh(3\Phi_L)} - \frac{1}{3\Phi_L})$$
 (24)

where Φ_L is the Thiele modulus which is given by:

Table 1The parameters used in the agglomerate scale and the fuel cell scale models.

| Parameter | value |
|---|---|
| Thickness of membrane (L_{mem}) | $3 \times 10^{-5} m$ |
| The thickness of the catalyst layer (L_{cl}) | $1.5 \times 10^{-5} m$ |
| Thickness of GDL (L_{GDL}) | $2.5 	imes 10^{-4} m$ |
| Cathode charge transfer coefficient (α_a) | 3.39 |
| Pressure (p) | 1.5atm |
| Temperature (T) | 353 K |
| Faradays' constant (F) | 96485Cmol ⁻¹ |
| Universal gas constant (R) | $8.314 \text{mol}^{-1} \text{K}^{-1}$ |
| Henry's constant (H) | 31664 Pa⋅m³mol ⁻¹ |
| Electrochemical active area of platinum particles (A_{pt}) | $40m^2g^{-1}[48]$ |
| Platinum loading (l_{pt}) | $4 	imes 10^{-3} Kg m^{-2}$ |
| Anode Exchange current density $(i_{0,a})$ | $100A m^{-2}$ |
| Cathode Exchange current density $(i_{0,c})$ | 0.015A m ⁻² [10] |
| Reference dissolved O_2 concentration $(c_{O_2}^{ref})$ | $0.85 \text{mol m}^{-3}[10]$ |
| Porosity of anode/cathode CL (ε_{cl}) | 0.48 |
| Porosity of anode/cathode GDL (ε) | 0.6 |
| Ionomer volume fraction in the agglomerate (ε_e) | 0.5 [10] |
| Oxygen diffusivity in the ionomer (D_e) | $8.45 \times 10^{-10} \text{m}^2 \text{s}^{-1} [46]$ |
| Oxygen in nitrogen diffusivity $(D_{O_2-N_2})$ | $1.86 \times 10^{-5} \text{m}^2 \text{s}^{-1} \text{[46]}$ |
| Oxygen in Water vapor diffusivity $(D_{O_2-H_2o})$ | $2.47\times 10^{-5}m^2s^{-1}\text{[46]}$ |
| Water vapor in nitrogen diffusivity $(D_{H_20-N_2})$ | $2.58\times 10^{-5}m^2s^{-1}\text{[46]}$ |
| Electric conductivity of gas diffusion layer (σ_{GDL}) | 100 S/m [10] |
| Electric conductivity of electrolyte (σ_m) | 0.8 S/m |
| Electric conductivity of catalyst layer (σ_{CL}) | 30 S/m [10] |
| Net drag coefficient (<i>nd</i>) | $\begin{aligned} &1(\eta<0.25V)\\ &46\eta^2-31.52\eta+5.7(0.25\leq\eta\leq0.35V)0.3\\ &(\eta>0.2V)\ [46] \end{aligned}$ |

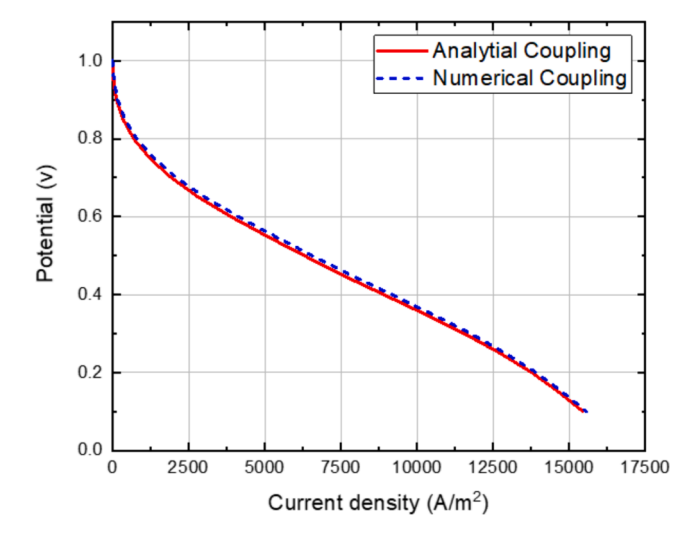


Fig. 7. The polarisation curves generated from the multi-scale model and the conventional agglomerate PEFC model. Note that, for the comparison to be valid, the case considered in the multiscale model is the case in which the core of the spherical agglomerate.

$$\Phi_L = \frac{r_{agg}}{3} \sqrt{\frac{k}{D_o^{eff}}}$$
 (25)

Fig. 7 shows that the polarisation curves as generated by: (i) the present multiscale modeling framework for the case in which the core of the agglomerate is assumed to be wholly chemically active and uniform (see Fig. 1 in [9]) and (ii) the conventional agglomerate model (represented by Equations (21–25)). The figure shows that the agreement between the two polarisation curves generated is very good. This provides confidence in the accuracy of the predictions of the multi-scale model developed in this study.

3.1. Catalyst agglomerate performance

Fig. 8 shows the performance curves obtained from the agglomerate scale models for the agglomerate with different sizes (100 and 1000 nm) and internal structure ("separate", "contacting" and "overlapping"). The first observation is that the catalyst agglomerate performs better with decreasing size. For example, for the agglomerate with a "separate" internal structure, the average volumetric current density increases by two orders of magnitude when decreasing the agglomerate radius from 1000 nm to 100 nm. This is attributed to the increased specific surface area with smaller agglomerates that enhances the availability of the active sites and subsequently leads to better catalyst utilisation. In other words, the reactant gas (which is oxygen in this case) is largely consumed as soon as it enters the active clusters in the agglomerate (particularly at high overpotential values) which means that most of the active region remains largely non-utilized (see Fig. 9); this phenomenon becomes more profound with larger catalyst agglomerates and leads to less volumetric current density by larger agglomerates.

The second observation is that, regardless of the agglomerate size, the agglomerates with separate active clusters perform better than the agglomerates with contacting active clusters and these agglomerates in turn perform better than those with overlapping active clusters. This is due to the fact that the total surface area is a maximum for the agglomerates with separate active clusters and a minimum with overlapping active clusters; the larger the surface area of the active area of the agglomerate, the better the utilization of the catalyst. As explained in Section 2, the graphs shown in Fig. 8 were used as interpolation functions for the PEFC scale model.

3.2. Fuel cell performance

Fig. 10 shows the polarisation curves of the modeled PEFC running with catalyst agglomerates of two sizes (100 and 1000 nm) and three different internal structures (separate, contacting and overlapping active clusters). As a general note, the fuel cell performs better with separate active clusters and this is evidently due to the larger specific area demonstrated by these active clusters (that allows for maximal exposure of the catalyst surface area to the reactant gases) compared to the other two active clusters. The second note is that the impact of the internal structure on the fuel cell performance becomes more significant when reducing the radius of the agglomerate from 1000 to 100 nm. For example, for the smaller agglomerates, the maximum current density with separate active clusters is larger than that with contacting active clusters by less than 1 %. On the other hand, for the larger agglomerates, the maximum current density with separate active clusters is larger than that with contacting active clusters by more than 12 %. These results are attributed to the increased diffusion paths (and subsequently the increased mass transport resistance) of the larger catalyst agglomerates compared to the smaller agglomerates; this translates into the fuel cell being more sensitive to changes in the internal structures, particularly in the high current density region where the fuel cell becomes more mass transport resistance limited. This sensitivity of the fuel cell performance to the agglomerate size is in accordance with those reported by Ismail

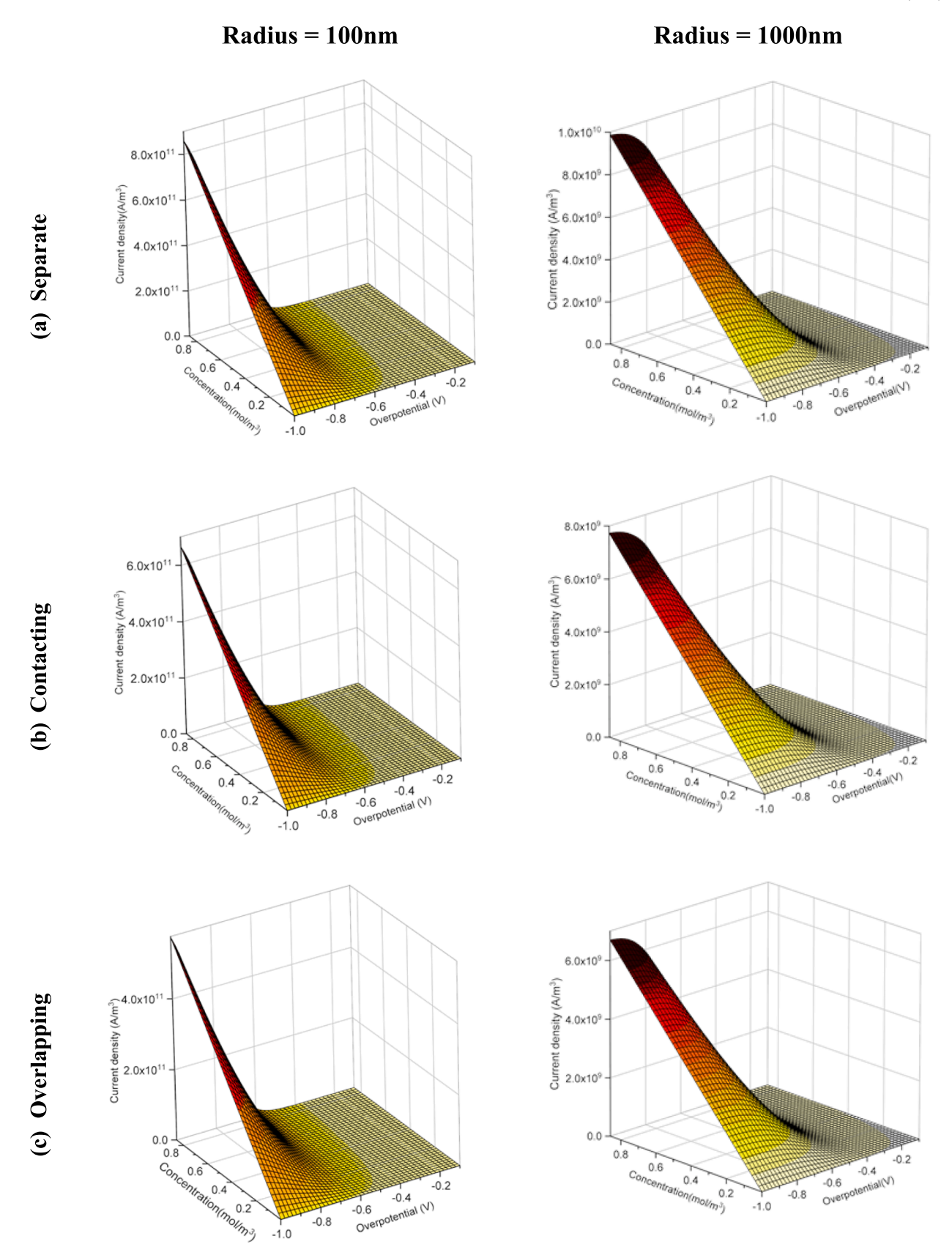


Fig. 8. The volumetric current density of the agglomerate as a function of activation overpotential and dissolved oxygen concentration for two agglomerate sizes (100 and 1000 nm) and three different internal structures (separate, contacting and overlapping active clusters).

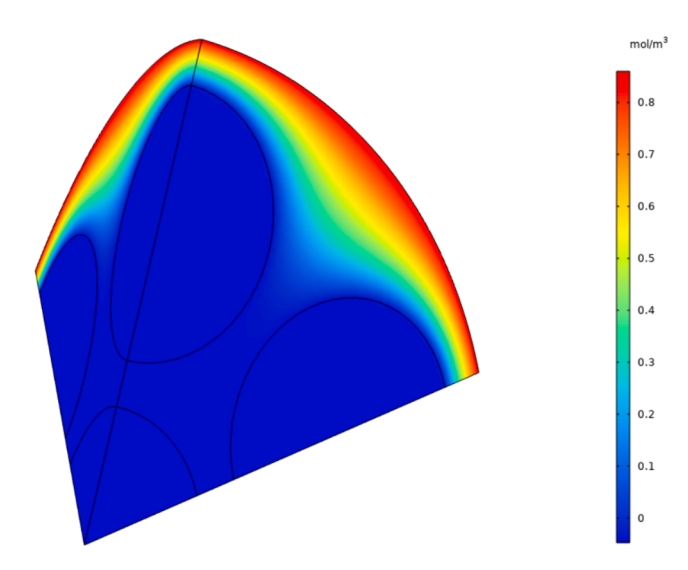


Fig. 9. The distribution of dissolved oxygen concentration at an activation overpotential of -1 within the modeled section of the catalyst agglomerate with 100 nm radius.

et al. [10] and Kamarajugadda et al. [36].

It is worth noting that, as inferred from Table 2, the agglomerates with separate active clusters not only improve the fuel cell performance but also reduce the amount of platinum catalyst. Namely, the total active volume of the agglomerate with separate active clusters is less than those with contacting and overlapping active clusters by around 20 and 45 %, respectively; this means that significantly less platinum catalyst is used when employing agglomerates with separate active clusters.

4. Conclusions and future works

A multiscale PEFC modeling framework has been developed. This framework consists of a catalyst agglomerate scale model and a fuel cell scale model. The agglomerate model is first solved to generate the performance plot which represents the average volumetric current density of the agglomerate as they change with dissolved oxygen concentration and activation overpotential. The above plot is used as an interpolation function that could be then linked to the fuel cell scale model to generate the local current density within the cathode catalyst layer for a given cell potential. This modeling framework has been used to investigate the impact of the internal structure of the catalyst agglomerate on the fuel

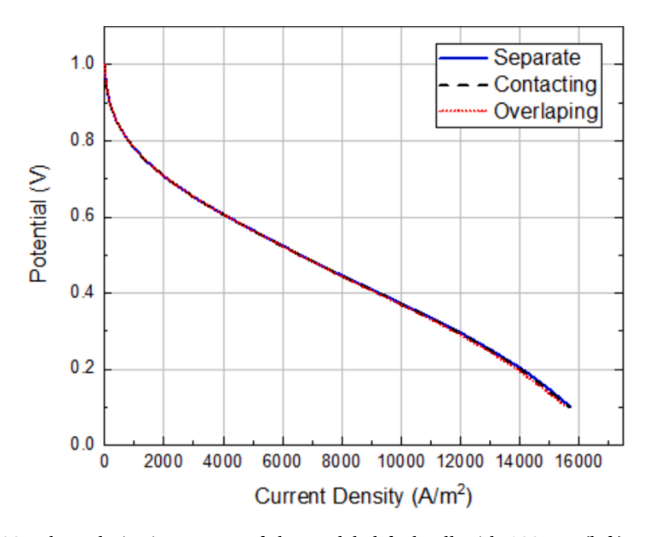
cell performance. This, given the massive advancement in microfabrication technologies, provides guidance for catalyst layer synthesis to enhance PEFC performance. For simplicity, the active clusters were assumed to be either separate from each other, contacting each other or overlapping each other. Below are the main findings:

- The fuel cell performs better with catalyst agglomerates featuring "separate" active clusters than those feature "contacting" or "overlapping" clusters and this is due to higher specific surface area demonstrated by the separate active clusters.
- This impact (i.e. the impact of the internal structure of the agglomerate on the fuel cell performance) becomes more profound as the size of the agglomerate increases. It was shown that the maximum current density with "separate" active clusters is larger than that with "contacting" active clusters by more than 12 % and this is because the fuel cell becomes more mass transport resistance limited with larger agglomerates.
- The modeled agglomerate performs better with decreasing size. The
 volumetric current density was found to increase by two orders of
 magnitude when catalyst agglomerate size decreased from 1000 nm
 to 100 nm. This is attributed to better catalyst utilization of the
 smaller agglomerates.
- Considering the current and future advancements in the nano- and micro-fabrication technologies, it is recommended to design catalyst agglomerates with "separate" active clusters as they improve the fuel cell performance and also reduce the catalyst loading.

The agglomerate model developed in this paper did not account for the influence of liquid water. Given that water generated during the cathode oxygen reduction reaction can significantly affect the reactant transport, future research should prioritise the development of more precise models that incorporate this aspect. Moreover, future efforts should be geared towards the creation of even more accurate three-dimensional-to-three-dimensional models. Ultimately, for long-term research goals, integrating experimental data into simulations has the potential to expedite the discovery and synthesis of catalysts that are not only more efficient but also more cost-effective.

Table 2The quantitive comparison of the volume of active area.

| | Separate | Contacting | Overlapping |
|-----------------------|----------|------------|-------------|
| $Va_i/Va_{spherical}$ | 0.38 | 0.53 | 0.63 |



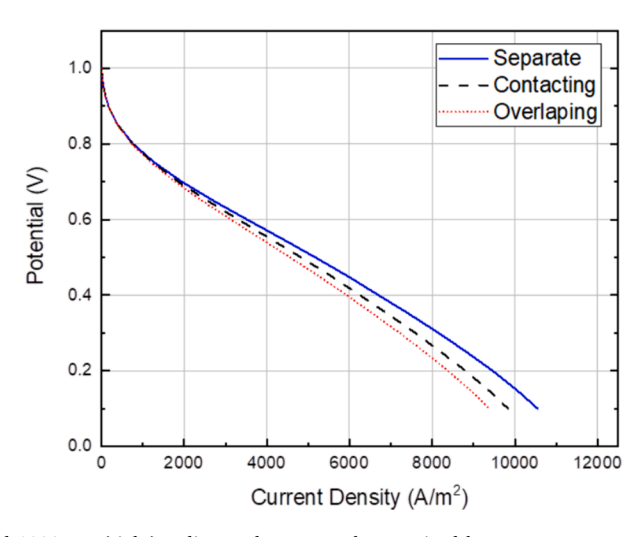


Fig. 10. The polarisation curves of the modeled fuel cell with 100 nm (left) and 1000 nm (right) radius agglomerates characterized by separate, contacting or overlapping active clusters.

CRediT authorship contribution statement

J. Tian: Writing – original draft, Visualization, Software, Resources, Project administration, Methodology, Investigation, Formal analysis, Data curation, Conceptualization. M.S. Ismail: Writing – review & editing, Supervision, Software, Resources, Methodology, Conceptualization. K.J. Hughes: Supervision. D.B. Ingham: Writing – review & editing, Supervision, Conceptualization. L. Ma: Supervision. M. Pourkashanian: Supervision.

Declaration of competing interest

The authors declare that they have no known competing financial interests or personal relationships that could have appeared to influence the work reported in this paper.

Data availability

No data was used for the research described in the article.

References

- [1] Calili-Cankir F, Ismail MS, Berber MR, Alrowaili ZA, Ingham DB, Hughes KJ, et al. Dynamic models for air-breathing and conventional polymer electrolyte fuel cells: a comparative study. Renew Energy 2022;195:1001–14. https://doi.org/10.1016/ i.renene.2022.06.092.
- [2] Ercelik M, Ismail MS, Ingham DB, Hughes KJ, Ma L, Pourkashanian M. Efficient X-ray CT-based numerical computations of structural and mass transport properties of nickel foam-based GDLs for PEFCs. Energy 2023;262:125531. https://doi.org/10.1016/j.energy.2022.125531.
- [3] Lee FC, Ismail MS, Ingham DB, Hughes KJ, Ma L, Lyth SM, et al. Alternative architectures and materials for PEMFC gas diffusion layers: a review and outlook. Renew Sustain Energy Rev 2022;166. https://doi.org/10.1016/j. rser 2022 112640
- [4] Okereke IC, Ismail MS, Ingham D, Hughes KJ, Ma L, Pourkashanian M. The effects of GDL anisotropic transport properties on the PEFC performance. Int J Numer Meth Heat Fluid Flow 2023;33:648–72. https://doi.org/10.1108/HFF-05-2022-0284.
- [5] Aldakheel F, Ismail MS, Hughes KJ, Ingham DB, Ma L, Pourkashanian M. Effects of compression on mechanical integrity, gas permeability and thermal stability of gas diffusion layers with/without sealing gaskets. Int J Hydrogen Energy 2021;46: 22907–19. https://doi.org/10.1016/j.ijhydene.2021.04.087.
- [6] Tian J, Ismail MS, Ingham D, Hughes KJ, Ma L. Multiphase, three-dimensional PEM fuel cell numerical model with a variable cross-sectional area flow channel. Int J Numer Meth Heat Fluid Flow 2023. https://doi.org/10.1108/HFF-02-2023-0075.
- [7] Litster S, Epting WK, Wargo EA, Kalidindi SR, Kumbur EC. Morphological analyses of polymer electrolyte fuel cell electrodes with nano-scale computed tomography imaging. Fuel Cells 2013;13:935–45.
- [8] Carton JG, Olabi AG. Three-dimensional proton exchange membrane fuel cell model: Comparison of double channel and open pore cellular foam flow plates. Energy 2017;136:185–95. https://doi.org/10.1016/j.energy.2016.02.010.
- [9] Fofana D, Natarajan SK, Hamelin J, Benard P. Low platinum, high limiting current density of the PEMFC (proton exchange membrane fuel cell) based on multilayer cathode catalyst approach. Energy 2014;64:398–403. https://doi.org/10.1016/j. energy.2013.10.021.
- [10] Ismail MS, Ingham DB, Ma L, Hughes KJ, Pourkashanian M. Effects of catalyst agglomerate shape in polymer electrolyte fuel cells investigated by a multi-scale modelling framework. Energy 2017;122:420–30. https://doi.org/10.1016/j. energy.2017.01.092.
- [11] Yang R, Liu Z, Liu J. The methodology of decoupling fuel and thermal nitrogen oxides in multi-dimensional computational fluid dynamics combustion simulation of ammonia-hydrogen spark ignition engines. Int J Hydrogen Energy 2024;55: 300–18. https://doi.org/10.1016/j.ijhydene.2023.09.105.
- [12] Liu J, Liu Z. In-cylinder thermochemical fuel reforming for high efficiency in ammonia spark-ignited engines through hydrogen generation from fuel-rich operations. Int J Hydrogen Energy 2024;54:837–48. https://doi.org/10.1016/j. ijhydene.2023.08.146.
- [13] Zheng X, Yang R, Wang Q, Yan Y, Zhang Y, Fu J, et al. Comparison of GRNN and RF algorithms for predicting heat transfer coefficient in heat exchange channels with bulges. Appl Therm Eng 2022;217. https://doi.org/10.1016/j.applthermaleng.2022.119263.
- [14] Antolini E. Carbon supports for low-temperature fuel cell catalysts. Appl Catal B 2009;88:1–24. https://doi.org/10.1016/j.apcatb.2008.09.030.
- [15] Esmaeilifar A, Rowshanzamir S, Eikani MH, Ghazanfari E. Synthesis methods of low-Pt-loading electrocatalysts for proton exchange membrane fuel cell systems. Energy 2010;35:3941–57. https://doi.org/10.1016/j.energy.2010.06.006.
- [16] Sasikumar JW, Ryu HGI. Dependence of optimum Nafion content in catalyst layer on platinum loading. J Power Sources 2004;132:11–7. https://doi.org/10.1016/j. jpowsour.2003.12.060.

- [17] Xie Z, Navessin T, Shi K, Chow R, Wang Q, Song D, Andreaus B, Eikerling M, Liu Z, Holdcroft S. Functionally graded cathode catalyst layers for polymer electrolyte fuel cells II. experimental study of the effect of nafion distribution. J Electrochem Soc 2005;152:1171–9. https://doi.org/10.1149/1.1904990.
- [18] Ismail M, Ingham D, Hughes KJ, Ma L, Pourkashanian M. The effects of shape on the performance of cathode catalyst agglomerates in polymer electrolyte fuel cells a micro-scale FEM study. Int J Numer Meth Heat Fluid Flow 2016;26:1145–56. https://doi.org/10.1108/HFF-10-2015-0416.
- [19] Siegel C. Review of computational heat and mass transfer modeling in polymerelectrolyte-membrane (PEM) fuel cells. Energy 2008;33:1331–52. https://doi.org/ 10.1016/j.energy.2008.04.015.
- [20] Djilali N. Computational modelling of polymer electrolyte membrane (PEM) fuel cells: challenges and opportunities. Energy 2007;32:269–80. https://doi.org/ 10.1016/j.energy.2006.08.007.
- [21] Kariuki NN, Myers DJ. To cite this article: Makoto Uchida et al. vol. 143. 1996.
- [22] Dou S, Hao L, Liu H. Effects of carbon aggregates and ionomer distribution on the performance of PEM fuel cell catalyst layer: A pore-scale study. Renew Energy 2023;217. https://doi.org/10.1016/j.renene.2023.119254.
- [23] Ünsal S, Bozzetti M, Chen Y-C, Girod R, Berger A, Diercks JS, et al. Catalyst aggregate size effect on the mass transport properties of non-noble metal catalyst layers for PEMFC cathodes. J Electrochem Soc 2023;170:074502. https://doi.org/ 10.1149/1945-7111/ace289.
- [24] Martens I, Chattot R, Drnec J. Decoupling catalyst aggregation, ripening, and coalescence processes inside operating fuel cells. J Power Sources 2022;521. https://doi.org/10.1016/j.jpowsour.2021.230851.
- [25] Song D, Wang Q, Liu Z, Navessin T, Eikerling M, Holdcroft S. Numerical optimization study of the catalyst layer of PEM fuel cell cathode. J Power Sources 2004;126:104–11. https://doi.org/10.1016/j.jpowsour.2003.08.043.
- [26] Marr Xianguo CL. Composition and performance modelling of catalyst layer in a proton exchange membrane fuel cell. J Power Sources 1999;77:17–27. https://doi. org/10.1016/s0378-7753(98)00161-x.
- [27] Secanell B, Suleman A, Djilali NMC. Numerical optimization of proton exchange membrane fuel cell cathodes. Electrochim Acta 2007;52:2668–82. https://doi.org/ 10.1016/j.electacta.2006.09.049.
- [28] Schwarz Nedjib DH, D.. 3D Modeling of Catalyst Layers in PEM Fuel Cells Effects of Transport Limitations. J Electrochem Soc 2007;154. https://doi.org/10.1149/ 1.2777011 (B1167-NA).
- [29] Jain LT, Jhon MSPB. Sensitivity of PEFC Models to Cathode Layer Microstructure. J Electrochem Soc 2010;157. https://doi.org/10.1149/1.3454725 (B1222-NA.).
- [30] Xing L, Liu X, Alaje T, Kumar R, Mamlouk M, Scott K. A two-phase flow and non-isothermal agglomerate model for a proton exchange membrane (PEM) fuel cell. Energy 2014;73:618–34. https://doi.org/10.1016/j.energy.2014.06.065.
- [31] Cetinbas FC, Advani SG, Prasad AK. Three dimensional proton exchange membrane fuel cell cathode model using a modified agglomerate approach based on discrete catalyst particles. J Power Sources 2014;250:110–9. https://doi.org/ 10.1016/i.jnowsour.2013.10.138.
- [32] Xing L, Cai Q, Xu C, Liu C, Scott K, Yan Y. Numerical study of the effect of relative humidity and stoichiometric flow ratio on PEM (proton exchange membrane) fuel cell performance with various channel lengths: an anode partial flooding modelling. Energy 2016;106:631–45. https://doi.org/10.1016/j. energy.2016.03.105.
- [33] Xing L, Du S, Chen R, Mamlouk M, Scott K. Anode partial flooding modelling of proton exchange membrane fuel cells: model development and validation. Energy 2016;96:80–95. https://doi.org/10.1016/j.energy.2015.12.048.
- [34] Pylypenko TS, Carroll NJ, Petsev DN, Atanassov PSO. Templated Platinum/Carbon Oxygen Reduction Fuel Cell Electrocatalysts. J Phys Chem C 2010;114:4200–7. https://doi.org/10.1021/jp909418m.
- [35] Balgis GM, Sago S, Ogi T, Okuyama KRA. Nanostructured design of electrocatalyst support materials for high-performance PEM fuel cell application. J Power Sources 2012;203:26–33. https://doi.org/10.1016/j.jpowsour.2011.11.064.
- [36] Kamarajugadda Sandip SM. Generalized flooded agglomerate model for the cathode catalyst layer of a polymer electrolyte membrane fuel cell. J Power Sources 2012;208:328–39. https://doi.org/10.1016/j.jpowsour.2012.02.063.
- [37] Moore M, Wardlaw P, Dobson P, Boisvert JJ, Putz A, Spiteri RJ, Secanell M. Understanding the Effect of Kinetic and Mass Transport Processes in Cathode Agglomerates. J Electrochem Soc 2014;161:E3125–37. https://doi.org/10.1149/ 2.010408ies
- [38] Mu YT, He P, Gu ZL, Qu ZG, Tao WQ. Modelling the reactive transport processes in different reconstructed agglomerates of a PEFC catalyst layer. Electrochim Acta 2022;404. https://doi.org/10.1016/j.electacta.2021.139721.
- [39] Larminie Andrew JD. Fuel cell systems explained. vol. NA. 2000. https://doi.org/ NA.
- [40] Siddique Fuqiang NA, L.. Process based reconstruction and simulation of a threedimensional fuel cell catalyst layer. Electrochim Acta 2010;55:5357–66. https:// doi.org/10.1016/j.electacta.2010.04.059.
- [41] Jinnouchi R, Kudo K, Kodama K, Kitano N, Suzuki T, Minami S, et al. The role of oxygen-permeable ionomer for polymer electrolyte fuel cells. Nat Commun 2021; 12. https://doi.org/10.1038/s41467-021-25301-3.
- [42] Middelman E. Improved PEM fuel cell electrodes by controlled self-assembly. Fuel Cells Bull 2002;2002:9–12. https://doi.org/10.1016/s1464-2859(02)11028-5.
- [43] Zlotorowicz A, Jayasayee K, Dahl PI, Thomassen MS, Kjelstrup S. Tailored porosities of the cathode layer for improved polymer electrolyte fuel cell performance. J Power Sources 2015;287:472–7. https://doi.org/10.1016/j. inovsour.2015.04.079
- [44] Suter TAM, Smith K, Hack J, Rasha L, Rana Z, Angel GMA, et al. Engineering catalyst layers for next-generation polymer electrolyte fuel cells: a review of

- design, materials, and methods. Adv Energy Mater 2021;11. https://doi.org/ 10.1002/aenm.202101025.
- [45] Wang M, Park JH, Kabir S, Neyerlin KC, Kariuki NN, Lv H, et al. Impact of catalyst ink dispersing methodology on fuel cell performance using in-situ X-ray scattering. ACS Appl Energy Mater 2019;2:6417–27. https://doi.org/10.1021/ acsaem.9b01037.
- [46] Sun BA, Karan KWP. An improved two-dimensional agglomerate cathode model to study the influence of catalyst layer structural parameters. Electrochim Acta 2005; 50:3359–74. https://doi.org/10.1016/j.electacta.2004.12.009.
- [47] Hao L, Moriyama K, Gu W, Wang C-Y. Modeling and Experimental Validation of Pt Loading and Electrode Composition Effects in PEM Fuel Cells. J Electrochem Soc 2015;162:F854–67. https://doi.org/10.1149/2.0221508jes.
- [48] Yoon AZ, Ww.. Modeling Low-Platinum-Loading Effects in Fuel-Cell Catalyst Layers. J Electrochem Soc 2011;158. https://doi.org/10.1149/1.3597644 (B1007-NA)
- [49] Ismail MS, Ingham DB, Hughes KJ, Ma L, Pourkashanian M. Effective diffusivity of polymer electrolyte fuel cell gas diffusion layers: an overview and numerical study. Int J Hydrogen Energy 2015;40:10994–1010. https://doi.org/10.1016/j. ijhydene.2015.06.073.